Characterising the short-term habituation of event-related evoked potentials

Flavia Mancini[1, 2,*], Alessia Pepe[3], Giulia Di Stefano[3],
André Mouraux[4], Gian Domenico Iannetti[1]

[1]*Department of Neuroscience, Physiology and Pharmacology, University College London, London, UK*
[2]*Computational and Biological Learning Lab, Department of Engineering, University of Cambridge, Cambridge, UK*
[3]*Department of Neurological Sciences, University of Rome 'La Sapienza', Rome, IT*
[4]*Institute of Neuroscience, Université Catholique de Louvain, Brussels BE*

* *Corresponding author:*
Flavia Mancini
University of Cambridge
Department of Engineering, Computational and Biological Learning Lab
Trumpington Street, Cambridge, CB2 1PZ
fm456@cam.ac.uk

Abstract

Fast-rising sensory events evoke a series of functionally heterogeneous event-related potentials (ERPs), which reflect the activity of both modality-specific and supramodal cortical generators overlapping in time and space. When stimuli are delivered at long and variable intervals (10-15 seconds), supramodal components appear as a large negative-positive biphasic deflection maximal at the scalp vertex (vertex wave) and dominate over modality-specific components. Stimulus repetition at 1 Hz induces a strong habituation of these supramodal components, which largely reflect stimulus saliency and behavioural relevance. However, the effect of stimulus repetition on lateralized modality-specific components is less clear. To comprehensively characterize how the different ERP waves habituate over time, we recorded the ERPs elicited by 60 identical somatosensory stimuli (either non-nociceptive Aβ or nociceptive Aδ), delivered at 1 Hz to healthy human participants. We show that the well-described spatiotemporal sequence of ERP components elicited by the first stimulus of the series is largely preserved in the smaller-amplitude, habituated response elicited by the last stimuli of the series. We also modelled the single-trial amplitude of the vertex wave elicited by the 60 Aβ and Aδ stimuli, and observed that it decays monotonically, with a largest drop of response magnitude at the first stimulus repetition, followed by much smaller decreases in subsequent repetitions. Altogether, these observations indicate that the main ERP constituents are preserved even when contextual modulations reduce the behavioural-relevance of the eliciting stimuli.

Significance

We comprehensively characterized the decay of event-related potentials (ERPs) elicited by identical fast-rising stimuli repeated at short and regular intervals (1Hz). Our observations indicate that, although response amplitude is reduced by stimulus repetition, the ERPs are obligatory contributed by both modality-specific lateralized components and supramodal vertex components. This indicates a fundamental and unavoidable property of the central nervous system: its sensitivity to respond to sudden changes in the environment with a transient synchronization of thalamocortical activity that manifests itself as widespread brain potentials detectable in the human EEG.

Introduction

Sudden sensory events evoke a series of transient responses in the ongoing electrocortical activity (event-related potentials, ERPs). ERPs are functionally heterogeneous and reflect the activity of distinct cortical generators overlapping in time and space (Sutton et al., 1965). Since these generators include both primary sensory and associative cortical areas, the scalp distribution of the ERPs elicited by stimuli of different modalities partly differs depending on the modality of the sensory input. However, when elicited by isolated and intense fast-rising stimuli, the activity of generators reflecting supramodal neural activities dominates over modality-specific activities (Liang et al., 2010). The scalp distribution of the electroencephalogram (EEG) signal reflecting supramodal generators is virtually identical regardless of the modality of the eliciting stimulus: it consists in a biphasic negative-positive deflection widespread over the scalp and maximal at the vertex – often referred to as 'vertex wave' or 'vertex potential' (Bancaud et al., 1953).

The vertex wave amplitude is maximal when fast-rising stimuli are presented using large and variable inter-stimulus intervals of several seconds (Mouraux and Iannetti, 2009; Huang et al., 2013), or when the stimulus reflects behaviourally relevant changes within a regular series of otherwise identical stimuli (Snyder and Hillyard, 1976; Valentini et al., 2011; Ronga et al., 2013). In contrast, when identical stimuli are monotonously repeated at short and regular intervals (e.g., 0.5 or 1 Hz), the vertex wave amplitude decays (Jasper and Sharpless, 1956; Ritter et al., 1968; Davis et al., 1972; Mouraux and Iannetti, 2009; Liang et al., 2010; Wang et al., 2010). For this reason, the vertex wave has been suggested to be related to the detection and immediate reaction to behaviourally-relevant, sudden events (Sutton et al., 1965; Mouraux and Iannetti, 2009), a hypothesis also supported by preliminary behavioural evidence (Wessel and Aron, 2013; Moayedi et al., 2016). The decay of the vertex wave due to repeated stimulation at different stimulation frequencies has been described already (Fruhstorfer et al., 1970; Greffrath et al., 2007). However, a full characterization of how the different constituent components of the ERP habituate over time is still missing.

Therefore, our primary objective was to describe the short-term habituation of the different components constituting somatosensory ERPs: both the large supramodal vertex waves and the smaller modality-specific lateralised waves. ERPs elicited by transcutaneous electrical stimulation of nerve trunks provide an excellent model to achieve this objective. Indeed, this stimulation activates directly all large-diameter Aβ somatosensory afferents, thus providing a synchronous volley that elicits cortical responses with a large signal-to-noise ratio. Furthermore, somatosensory ERPs are well characterised in terms of deflections, topographies and underlying generators.

We recorded EEG while delivering trains of 60 identical Aβ stimuli at 1 Hz. We characterized the ERP habituation in three complementary ways. First, we statistically assessed the presence of the main response components in both the non-habituated ERP (i.e. the ERP elicited by the first stimulus of a series) and the habituated ERP (i.e. the ERP elicited by later stimuli that elicit a stable, habituated response). The rationale for this decision consists in the consistent observation that the amplitude of the main ERP waves decays only minimally after the first few stimulus repetitions (Ritter et al., 1968; Fruhstorfer et al., 1969; Fruhstorfer et al., 1970; Fruhstorfer, 1971; Greffrath et al., 2007; Mouraux et al., 2013), a finding corroborated by the present results (Figures 1-3). Second, we fitted a number of functions derived from previous studies (Fruhstorfer et al., 1970; Greffrath et al., 2007), to model the

time-profile of the decay of the supramodal ERP components (the negative and positive vertex waves). Finally, we used probabilistic independent components analysis (pICA) (Mouraux and Iannetti, 2009) to effectively break down both the non-habituated ERP and the habituated ERP into functionally-independent components. To cross-validate and generalise our findings across different sensory pathways, we replicated the experiment in a separate group of healthy participants, using radiant-heat stimuli that selectively activate skin nociceptors and elicit sensations of Aδ-mediated pinprick pain.

Methods

Participants

Thirty-two healthy subjects (14 women) aged 19–31 years (mean ± SD: 23.6 ± 3.9) participated in the study, after having given written informed consent. All experimental procedures were approved by the ethics committee of University College London (2492/001).

Transcutaneous electrical stimulation of Aβ fibers

Innocuous stimulation of Aβ afferents consisted of square-wave pulses (100 μs duration), generated by a constant current stimulator (DS7A, Digitimer, UK). Stimuli were delivered through a bipolar electrode placed above the superficial radial nerve, and elicited a paresthetic sensation in the corresponding innervation territory. Aβ detection thresholds were identified using the method of ascending staircases, on the right hand. The detection threshold was defined as the average of the lowest stimulus energy eliciting a sensation in 3 consecutive trials. Electrical stimuli were delivered at approximately 300% of each individual's Aβ detection threshold. Stimulus intensity was slightly adjusted to elicit sensations of comparable intensities on the left and right hands (mean ± SD, 17.4 ± 11.4 mA) and to make sure that the elicited sensation was never painful.

Cutaneous laser stimulation of Aδ and C fibers

Nociceptive stimuli were radiant heat pulses generated by an infrared neo-dymium:yttrium-aluminum-perovskite laser with a wavelength of 1.34 μm (Nd:YAP; Electronical Engineering, Italy). At this wavelength, laser pulses excite Aδ and C nociceptive free nerve endings in the epidermis directly and selectively, i.e. without coactivating touch-related Aβ fibers in the dermis (Bromm and Treede, 1984; Baumgartner et al., 2005; Mancini et al., 2014). The duration of each laser pulse was 4 ms.

Laser stimuli were delivered within a squared skin area (4 x 4 cm) centered on the dorsum of the hand, encompassing the area in which the stimulation of Aβ afferents elicited the paresthesia. The laser beam was transmitted through an optic fiber, and its diameter at target site was set at ~6 mm by focusing lenses. A visible He–Ne laser pointed to the stimulated area.

The method of ascending staircases used for identifying the detection threshold of Aβ stimuli was also used to identify the detection threshold of Aδ stimuli. For the EEG recordings, the stimulus energy was clearly supra-threshold for Aδ fibers (0.53 ± 0.06 J/mm^2). This stimulus energy elicited intense but tolerable pinprick pain sensations, of comparable intensities on the right and left hands. Because

variations in baseline skin temperature may modulate the intensity of the afferent nociceptive input (Iannetti et al., 2004), an infrared thermometer was used to ensure that the hand temperature varied no more than 1°C across blocks. To avoid receptor fatigue or sensitization, the laser beam was displaced after each stimulus by ~1 cm within the predefined stimulated area.

Experimental procedure

Participants sat comfortably with their hands resting on a table in front of them. They were instructed to focus their attention on the stimuli, and fixate a yellow circular target (diameter: 1 cm) placed in front of them at a distance of approximately 60 cm from their face. A black curtain blocked the view of the hands. Throughout the experiment, white noise was played through headphones, to mask any sound associated with the either type of somatosensory stimulation.

The experiment was performed on 32 participants, divided in two groups of 16 participants. One group received electrical stimuli, and the other group received laser stimuli, using an identical procedure. Each participant received the somatosensory stimuli in 10 blocks, separated by a 5-minute interval, during which participants were allowed to rest. Each block consisted of 60 somatosensory stimuli delivered at 1 Hz: thus, each block lasted 1 minute. In each block, stimuli were delivered either to the right hand or to the left hand. Right- and left-hand blocks were alternated. The order of blocks was balanced across participants; half of the subjects started with a right-hand block, and the other half started with a left-hand block. At the end of each block, participants were asked to provide an average rating of perceived stimulus intensity, using a numerical scale ranging from 0 ("no sensation") to 10 ("most intense sensation"). This was done to ensure that the perceived intensity of the stimuli was similar across blocks (rating variability (SD) across blocks: electrical stimuli, 0.2 ± 0.2; laser stimuli: 0.3 ± 0.4).

Electrophysiological recordings

EEG was recorded using 30 Ag–AgCl electrodes placed on the scalp according to the International 10-20 system, using the nose as reference. Electrode positions were 'Fp1', 'Fpz', 'Fp2', 'F7', 'F3', 'Fz', 'F4', 'F8', 'T3', 'C3', 'Cz', 'C4', 'T4', 'T5', 'P3', 'Pz', 'P4', 'T6', 'O1', 'Oz', 'O2', 'FCz', 'FC4', 'FC3', 'Cp3', 'Cp4'. Eye movements and blinks were recorded from the right *orbicularis oculi* muscle, using 2 surface electrodes. The active electrode was placed below the lower eyelid, and the reference electrode a few centimeters laterally to the outer canthus. Signals were amplified and digitized using a sampling rate of 1,024 Hz (SD32; Micromed, Italy).

EEG analysis

1. Preprocessing. EEG data were preprocessed and analyzed using Letswave 6 (http://www.nocions.org/letswave/) and EEGLAB (https://sccn.ucsd.edu/eeglab/). Continuous EEG data were band-pass filtered from 0.5 to 30 Hz, segmented into epochs using a time window ranging from -0.2 to 0.8 sec relative to the onset of each stimulus, and baseline corrected using the interval from -0.2 to 0 sec as reference. Trials contaminated by large artifacts (<10% in each block) were removed. Eye blinks and movements were corrected using a validated method based on Independent Component Analysis (Jung et al., 2000). In all datasets, independent components related to eye movements showed a large EOG channel contribution and a frontal scalp distribution. To allow

averaging across blocks while preserving the possibility of detecting lateralized EEG activity, scalp electrodes were flipped along the medio-lateral axis for all signals recorded in response to left hand stimulation.

2. Statistical assessment of ERP components. To assess the consistency of stimulus-evoked modulations of EEG amplitude across time, we performed a one-sample t-test against zero (i.e. against baseline) for each electrode and time point of the entire waveform, a procedure yielding a scalp distribution of t-values across time. This analysis was performed separately on the non-habituated ERP and on the habituated ERP. The non-habituated ERP was derived by averaging all the responses elicited by the 1st stimulus of all blocks. The habituated ERP was derived by averaging the responses elicited by the 6th to the 60th stimuli of all blocks. The decision of using these responses elicited by stimuli 6th to 60th as a proxy of the habituated ERP was based on the observation that the amplitude of the main ERP waves decays only minimally after the first 5 stimulus repetitions (Figure 1, 3), as already described (Fruhstorfer et al., 1970; Greffrath et al., 2007). Figures 1 and 3 show how the amplitude of the ERPs was consistently habituated after the first few stimulus repetitions.

3. Modelling the within-block decay of the vertex waves. Given the large amplitude of the supramodal vertex waves contributing to the ERP, we were able to characterize their trial-by-trial variability in both amplitude and latency, across the 60 stimuli of each block. We tested whether the N2 and P2 peaks of both the Aβ- and Aδ-evoked vertex waves decayed following different functions derived from previous studies (Fruhstorfer et al., 1970; Greffrath et al., 2007). In each participant, we first averaged each of the 60 ERP responses across the 10 recording blocks, and thus obtained 60 average ERP waveforms: one for each of the 60 trials. On these averages, we measured the single-trial latency and amplitude values of the 60 N2 and P2 peaks at Cz, using a validated procedure based on multiple linear regression (Hu et al., 2010; Hu et al., 2011). Finally, we averaged the extracted peaks across participants, and modelled the decay of the N2 and P2 peak amplitudes across the 60 trials, using three different equations:

$$(1) \qquad y = a + \frac{b}{x}$$

$$(2) \qquad y = a + \frac{b}{x^c}$$

$$(3) \qquad y = a + e^{-bx}$$

where y is the peak amplitude of the N2 or P2 wave, x is the trial number (from 1 to 60), e is the Euler constant, and a, b, c are the parameters to be estimated using a least squares method. We tested these specific models of ERP decay given the previous evidence that the vertex wave decays sharply at the first stimulus repetition (Fruhstorfer et al., 1970; Greffrath et al., 2007; Mouraux and Iannetti, 2009; Valentini et al., 2011; Ronga et al., 2013). No constraints were set on the parameters to be estimated. The decay of the N2 and P2 components was modelled separately, because these waves can be independently modulated (Legrain et al., 2002; Hatem et al., 2007). To compare which model best fitted the data, we calculated the adjusted r^2 and the Akaike information criterion of each model, corrected for low sample size (AICc). The AIC is a relative estimate of the information lost in a given model, and it allows a fair comparison between non-linear models of different complexity, i.e. even when they have a different number of parameters. The lower the AIC, the better the model represents the measured data. From the difference in AICc values, we calculated the probability that each model was correct, with the probabilities summing to 100% (Burnham and Anderson, 2002). Finally, we tested for equal

variance of the residuals using the 'test for appropriate weighting', as implemented in Prism GraphPad 7.0.

4. Blind source separation using Probabilistic-ICA (pICA). To decompose ERPs in functionally independent components, we performed a validated blind source separation using an Independent Component Analysis (ICA; (Makeig et al., 1997) constrained to an effective estimate of the intrinsic dimensionality of the original data (probabilistic ICA, pICA) (Beckmann and Smith, 2004; Mouraux and Iannetti, 2009; Liang et al., 2010).

When applied to multi-channel EEG recordings, unconstrained ICA separates the signals recorded on the scalp into a linear combination of independent components (ICs), each having a fixed scalp topography and a maximally independent time course. When ICA is unconstrained, the total number of ICs equals the total number of recording electrodes. If the number of ICs differs greatly from the actual number of independent sources contributing to the signal, this may constitute a critical problem (Beckmann and Smith, 2004). Indeed, if the number of ICs is much larger than the number of sources, ICs containing spurious activity will appear because of overfitting. On the contrary, if the number of ICs is much smaller than the number of sources, valuable information will be lost due to under-fitting.

The problem of overfitting could be particularly important when unconstrained ICA is applied to averaged ERP waveforms. Because the averaging procedure cancels out sources of activity unrelated to the stimulus (e.g. ongoing EEG activity, muscular activity and noise), the number of independent sources present in the average waveform may be far smaller than the number of independent sources present in the original EEG signal.

These fundamental limitations can be addressed using pICA, in which the number of ICs is constrained to an effective estimate of the number of independent sources contributing to the original data (Beckmann and Smith, 2004). The number of independent sources was estimated using a method based on maximum likelihoods, and operating on the eigenvalues of a Principal Component Analysis (Rajan and Rayner, 1997).

pICA was conducted on the signals averaged across subjects, and was performed separately on the non-habituated ERP (trial #1) and on the habituated ERP (average of trials #6-60; see "*Statistical assessment of ERP components*" for the rationale behind this choice). pICA was also conducted on the concatenated non-habituated and habituated ERP, i.e. on the average ERP waveform from trial #1 concatenated to the average ERP waveform from trials #6-60.

Results

Response waveforms and topographies

Group-average ERPs elicited by Aβ and Aδ stimuli are shown in Figures 1 and 2. As expected, the latency of Aδ-ERPs was longer than the latency of Aβ-ERPs, because Aδ fibers are thinly myelinated and thus have slower conduction velocity than large-myelinated Aβ fibers (Mountcastle, 2005). The overall ERP amplitude dramatically decreased after the very first stimulus repetition, in both stimulus

modalities. Figure 2 shows that, both in the non-habituated response (trial #1) and in the habituated response (average of trials #6-60), the ERP was composed by the supramodal negative and positive vertex wave, as well as by the early and late somatosensory lateralised waves (N1 and P4, respectively) (Hu et al., 2014; Mancini et al., 2015). Expectedly, the response elicited by trial 1 had a clearly larger magnitude and a slightly longer latency than the average response in trials 6-60, for both the Aβ and the Aδ response. A statistical assessment of these responses is presented in Figure 2: in all stimulus modalities and condition, both vertex and lateralised responses were greater than baseline.

Modelling the decay of the vertex wave elicited by stimuli repeated at 1 Hz

Figure 3 shows the inter-individual variability in amplitude and latency of the N2 and P2 peaks, for each of the 60 trials, as well as the fit of the three models we tested. We found that the same model best predicted the decay of both Aβ and Aδ responses. This winning model was equation #2, and the decay of the four peaks was described as follows:

$$\text{Aβ N2} = -4.22 - \frac{19.37}{x^{1.46}}$$

$$\text{Aβ P2} = 9.12 + \frac{14.52}{x^{1.35}}$$

$$\text{Aδ N2} = -5.01 - \frac{14.03}{x^{2.05}}$$

$$\text{Aδ P2} = 8.34 + \frac{14.37}{x^{2.51}}$$

where x is the trial number.

The probability of model #2 fitting the data better than models #1 and #3 was higher than 99.99%. The AICc was always smallest in model #2. The difference in AICc between equation #2 and #1 was -20.3 for Aβ-N2, -7.4 for Aβ-P2, -21.5 for Aδ-N2, and -22.6 for Aδ-P2; the difference in AICc between equation #2 and #3 was more pronounced: -146.0 for Aβ-N2, -115.3 for Aβ-P2, -85.7 for Aδ-N2, and -68.2 for Aδ-P2. The adjusted r^2 of the winning model #2, another measure of goodness of fit, were 0.92 (Aβ-N2), 0.87 (Aβ-P2), 0.79 (Aδ-N2), and 0.72 (Aδ-P2). Lastly, the residuals of the winning models were homoscedastic ($p > 0.999$).

In qualitative terms, winning model #2 indicates that the amplitude of the examined peaks decays monotonically, with a fastest and sharpest drop of response magnitude at the first stimulus repetition, followed by much smaller decreases in the subsequent repetitions.

Functional decomposition of Aβ and Aδ ERPs elicited by stimuli repeated at 1 Hz

The functional decomposition of Aβ and Aδ ERPs are presented in Figures 4 and 5, for the non-habituated response (top panels), the habituated response (middle panels), and the concatenated non-habituated and habituated response (bottom panels). These figures show the topographic distribution of each independent component (IC), ranked according to the percentage of explained variance, together with their contribution to the ERPs at channel Cz and to the EEG global field power (GFP).

Aβ-ERPs. pICA identified five ICs in the ERP elicited by stimulus 1 (Figure 4A), and five ICs in the ERP elicited by the average of stimuli 6-60 (Figure 4B).

In the ERP elicited by stimulus 1, IC #1 and #2 explained the majority of the P2 wave (GFP peak latencies: 241 and 293 ms), and were centrally distributed, with a maximum over the vertex electrodes. IC #3 and #4 explained the majority of the N2 wave (peak latencies: 113 and 143 ms), although their distribution was not fully centred on the scalp vertex. IC #5 contributed to both the earliest and the latest part of the ERP time-course, and likely reflected lateralised responses (peak latencies: 67 and 347 ms). Accordingly, its scalp distribution was contralateral to the stimulated hand. Both the scalp distribution and the timecourse of these components match well previous blind source separation of ERPs elicited by intense and isolated somatosensory stimuli (Liang et al., 2010).

In the ERP elicited by stimuli 6-60, IC #1 explained the majority of the P2 wave (GFP peak latency: 238 ms), whereas IC #2 explained the majority of the N2 wave (peak latency: 135 ms). IC #3 isolated EEG activities contralateral to the stimulated hand, occurring in both early and late time windows of the signal (peak latencies: 112 and 389 ms). Therefore, the neural activity isolated by IC #3 are likely to correspond to the N1 and P4 waves of somatosensory ERPs.

To further assess whether the same components contributed to the non-habituated and habituated ERP waves, we performed a pICA on the concatenated ERP waveforms elicited by stimulus 1 and by the average of stimuli 6-60. This analysis identified five ICs (Figure 4C). IC #1 was symmetrically distributed over the vertex and explained the vast majority of the N2 wave in both the non-habituated and habituated response, as well as part of the P2 wave in the non-habituated ERP. IC #2 was also maximal over Cz, and contributed to the majority of the P2 wave in the response elicited by both stimulus 1 and stimuli 6-60. No single IC unequivocally isolated neural activities corresponding to the lateralised N1 and P4 waves shown in Figure 2.

Aδ-ERPs. Probabilistic ICA identified six ICs from the EEG responses to stimulus 1, and four ICs from the EEG responses to the average of stimuli 6-60 (Figure 5).

In the ERP elicited by stimulus 1, IC #1 and #2 had the typical topographical distribution of a vertex wave: IC #1 explained the majority of the P2 wave (GFP peak latency: 347 ms), and IC #2 explained the majority of the N2 wave (peak latency: 185 ms). IC #3 had a central-parietal distribution contralateral to the stimulated hand, and clearly reflected the late P4 wave observed in laser ERPs (peak latency: 423 ms) (Hu et al., 2014; Mancini et al., 2015). Probably because of the low signal-to-noise ratio consequent to the small number of stimulus repetitions, no IC unequivocally explained the early contralateral neural activity.

In the ERP elicited by stimuli 6-60, IC #1 was again centrally and symmetrically distributed and explained the majority of the P2 wave (peak latency: 307 ms). IC #2 had a contralateral central-parietal distribution contralateral to the stimulated hand, and explained the P4 wave (peak latency: 389 ms). ICs #3 had a maximal distribution over Cz and C3, and contributed to both the N1 and N2 waves (peak

latency: 196 ms), possibly because of underfitting. IC #4 had a distribution contralateral to the stimulated hand and explained the early part of the N1 wave (peak latency: 138 ms).

pICA performed on the concatenated non-habituated and habituated ERP waves identified six ICs (Figure 5C). IC #1 and #2 were symmetrically distributed over the vertex. They explained the majority of the P2 wave (IC #1) and N2 wave (IC #2) in the response elicited by both stimulus 1 and stimuli 6-60. IC #3 had a maximal distribution over Pz and P3, and explained the early N1 wave and part of the late P4 modality-specific waves, both in the non-habituated and habituated response. Finally, IC #4 had maximal distribution over C3, Cz, and C4, and explained a late positive wave in the response to both stimuli 1 and 6-60.

In conclusion, irrespectively of amplitude differences, the spatiotemporal pattern of the evoked brain activity was largely similar not only for Aβ-ERPs and Aδ-ERPs (Treede et al., 1988), but also for the response elicited by stimulus 1 and stimuli 6-60.

Discussion

In this study, we formally characterise the ERP habituation induced by repeating 60 identical somatosensory stimuli (both non-nociceptive, Aβ, and nociceptive, Aδ) at 1 Hz. Although the response amplitude was clearly reduced, the spatiotemporal sequence of the ERP waves was overall preserved in the habituated response (Figures 2, 4-5). This was substantiated by point-by-point statistical analysis as well as probabilistic ICA: both somatosensory-specific and supramodal components of the ERP elicited by sporadic and unpredictable stimuli (Liang et al., 2010; Hu et al., 2014; Mancini et al., 2015) also contributed to the habituated ERP elicited by frequent and predictable stimuli.

Effect of stimulus repetition on supramodal ERP responses

The negative-positive vertex wave (VW) is the largest component of the EEG response elicited by sudden sensory stimuli. Its high signal-to-noise ration makes the VW amplitude measurable in single trials, even when the response is habituated by stimulus repetition. Therefore, we were able to estimate the amplitude of the negative (N2) and positive (P2) vertex waves for each of the 60 ERPs (Figure 3). The decay of the negative and positive peaks was best modelled as follows:

$$y = a + \frac{b}{x^c}$$

where y is the peak amplitude of the N2 or P2 wave, x is the trial number, and a, b, c are the estimated parameters. This indicates that the amplitude of both vertex waves decays monotonically, with a largest, transient drop of response magnitude at the first stimulus repetition, followed by much smaller decreases in subsequent repetitions.

Converging evidence indicates that stimuli of virtually all sensory modalities can elicit a VW, provided that they are salient enough (Liang et al., 2010). It is therefore not surprising that the VW elicited by auditory stimuli repeated at 1-Hz decays following a function similar to the one observed here for somatosensory stimuli (Fruhstorfer et al., 1970). Even when considering experimental observations that did not formally model the response habituation, the maximum decrease in VW amplitude consistently occurs at the first stimulus repetition, for auditory (Ritter et al., 1968; Fruhstorfer et al., 1970),

somatosensory (Larsson, 1956; Fruhstorfer, 1971; Iannetti et al., 2008; Wang et al., 2010; Valentini et al., 2011; Ronga et al., 2013) and visual stimuli (Courchesne et al., 1975; Wastell and Kleinman, 1980). The similarity of the decay of the VW elicited by Aβ and Aδ stimuli (Figure 3) further confirms the multimodal nature of the neural generators of these signals (Mouraux and Iannetti, 2009). The mechanisms underlying such sharp reduction of response amplitude at the first stimulus repetition are likely to be similar across sensory systems.

Before discussing the contribution of the present results in elucidating the functional significance of the VW, it is important to highlight the empirical evidence that the observed response habituation is not due to neural refractoriness of afferent neurons or to fatigue of primary receptors. A previous study recorded ERPs elicited by pairs of nociceptive stimuli delivered at short intervals, which could either be identical or variable across the block (Wang et al., 2010). Only when the inter-stimulus interval was *constant* across the block, the VWs elicited by the second stimulus were reduced in amplitude. The peak amplitude of the VWs elicited by the second stimulus was instead as large as the VWs elicited by the first stimulus when the inter-stimulus interval was *variable*, indicating that neither neural refractoriness nor fatigue can easily explain the sharp response decay to stimulus repetition.

Furthermore, if the sharp response habituation at the first stimulus repetition was determined by fatigue of primary sensory receptors, we would have observed different decay profiles for stimuli delivered in varying vs constant spatial locations. Indeed, the VW elicited by contact heat stimuli at long and variable intervals (8-10 seconds) decays much faster if the second stimulus is delivered at the same spatial location of the first (Greffrath et al., 2007). Instead, we observed remarkably similar patterns of ERP decay for both Aδ laser stimuli delivered at different spatial locations and Aβ electrical stimuli delivered in the same skin region. Additionally, electrical stimuli activate directly the axons in the nerve trunk, bypassing the receptor, further ruling out receptor fatigue as explanation for the Aβ-ERP habituation. Receptor fatigue might still contribute to the slow decrease in ERP magnitude observed across dozens of stimulus repetitions of laser stimuli (Greffrath et al., 2007), but certainly not to the dramatic reduction of ERP amplitude we observed after one single stimulus repetition.

The physiological significance of the VW remains to be properly understood. However, there is evidence that this large electrocortical response reflects neural activities related to the detection of salient environmental events (Jasper and Sharpless, 1956; Mouraux and Iannetti, 2009) and execution of defensive movements (Moayedi et al., 2016). The detection of salient events relies on a hierarchical set of rules that consider both their probability of occurrence and their defining basic features (Legrain et al., 2002; Wang et al., 2010; Valentini et al., 2011; Ronga et al., 2013). The present results are informative with respect to this functional framework. Indeed, stimulus repetition did not abolish the VW elicited by either Aβ or Aδ stimuli, although it reduced its amplitude already after the first stimulus repetition. Therefore, even when stimulus saliency is reduced by contextual factors, there is a residual activity of the VW generators, only minimally reduced after the first few stimulus repetitions (Figures 1, 3). These findings point towards the existence of an obligatory VW activity triggered by any sudden and detectable change in the environment, even when contextual modulations minimize its behavioural relevance.

Extensive evidence from cell physiology indicates that neural habituation to repeated stimuli arises from alterations of synaptic excitability. Even the simple gill-withdrawal reflex in Aplysia dramatically

habituates at the first stimulus repetition (Byrne et al., 1978), due to a decreased drive from the sensory neurons onto follower motor neurons (Castellucci et al., 1970; Carew and Kandel, 1973). The temporal profile of this short-term habituation follows a fast decay function (Carew and Kandel, 1973), strikingly similar to that observed in this and other studies on the habituation of electrocortical responses in humans (Fruhstorfer et al., 1970; Greffrath et al., 2007). These synaptic changes have been interpreted as a hallmark of learning, and are central to the ability of the nervous system to adapt to environmental events (Carew and Kandel, 1973). Interpreting the decay of neural responses as functionally relevant for learning is not in contradiction with attentional interpretations: stimuli that are learned and recognized are likely to require less attentional resources than novel stimuli, and stimuli that need to be learned are typically more salient.

Effect of stimulus repetition on somatosensory lateralized responses

In somatosensory ERPs, the VW is both preceded and followed by other deflections of smaller amplitude. These have a topographical distribution maximal over centro-parietal electrodes in the hemisphere contralateral to hand stimulation. The earliest negative wave is usually referred to as N1 (Valentini et al., 2012) and the latest positive waveform of somatosensory ERPs is referred to as P4 (Hu et al., 2014; Mancini et al., 2015). Whereas the P4 has only been recently identified and its significance is not yet understood, the N1 has been replicated in a large body of studies (Spiegel et al., 1996; Garcia-Larrea et al., 2003; Lee et al., 2009; Hu et al., 2014; Mancini et al., 2015), and reflect somatosensory-specific neural activities more obligatorily related to the incoming afferent input (Lee et al., 2009; Liang et al., 2010). Both N1 and P4 are likely to originate in the primary somatosensory cortex (Valentini et al., 2012; Hu et al., 2014).

We showed that these modality-specific N1 and P4 responses are detectable not only in the response to the first stimulus, but also in the habituated response, as supported by the statistical assessment of the scalp distribution of the ERP response elicited by both the first and the last stimuli of the series (Figure 2). This is important, given that a previous study using trains of intra-epidermal electrical shocks at 1 Hz failed to observe any lateralized response (Mouraux et al., 2013). It is difficult to reconcile these two different observations, and we can only speculate about why that previous experiment failed to detect lateralised responses in the habituated response. One possibility is that intra-epidermal electrical stimulation causes a stronger peripheral and perceptual habituation, more significant than for radiant heat stimulation (Mouraux et al., 2010).

Conclusion

Our results provide a comprehensive functional characterization of the decay of ERPs when identical somatosensory stimuli are repeated at 1Hz. Fast-rising stimuli elicit ERPs obligatory contributed by both modality-specific and supramodal neural activities, even when the stimulus repetition minimizes stimulus relevance. This indicates a fundamental and compulsory property of the nervous system: its sensitivity to respond to sudden changes in the environment with a transient synchronization of thalamocortical activity that manifests itself as widespread brain potentials detectable in the human EEG.

Figure captions

Figure 1. *Habituation of the ERPs elicited by repeated Aβ (left panel) and Aδ (right panel) stimuli.* The figure shows the ERPs elicited by 60 stimuli delivered at 1 Hz, at electrode Cz referenced to the nose (vertex waves). The responses to both the first five stimuli and the last five stimuli are enlarged and presented super-imposed, to facilitate visual comparison.

Figure 2. *Habituation of supramodal vertex waves (N2, P2) and lateralized responses (N1, P4) elicited by Aβ (top panel) and Aδ (right panel) somatosensory stimuli.* Displayed signals show group-level ERPs recorded from the vertex (Cz vs nose) and from the central electrode contralateral to the stimulated hand (Cc vs Fz), elicited by the first stimulus in a series (non-habituated response) and by the average of trials #6-60 (habituated response). Scalp topographies are displayed at the peak latency of the N1, N2, P2, and P4 waves, in all conditions. To assess the consistency of stimulus-evoked modulations of ERP amplitude across time, we performed a one-sample *t*-test against zero (i.e. against baseline) for each electrode and time point of the waveform. Point-by-point *t* values are shown below the ERPs. Time intervals during which the ERP waves were significantly different than 0 in the N1, N2, P2, and P4 time windows are highlighted in orange.

Figure 3. *Modeling the decay of the vertex wave elicited by repeated Aβ (left panels) and Aδ (right panels) stimuli.* The average peak amplitudes (top panels) and latencies (bottom panels) of the N2 (blue circles) and P2 (yellow circles) components of the vertex wave are displayed for each of the 60 trials. The function that best fit the decay of response amplitude (equation #2 in the main text, here indicated by the arrow) is displayed with a black line.

Figure 4. *Functional decomposition of the Aβ-ERP elicited by the first stimulus (A, top-panel), by the average of stimuli 6-60 (B, middle panel), and of the concatenated Aβ-ERP elicited by stimulus 1 and 6-60 (C, bottom panel).* The top row of each panel shows the scalp topographies of the Independent Components (ICs), identified by the probabilistic Independent Component Analysis (pICA). The middle row of each panel shows the signals obtained by back-projecting each IC (thick colored waveforms) onto channel Cz. The original ERP waveforms at Cz is shown as a thin and grey line. The bottom row of each panel shows the contribution of each IC to the global field power.

Figure 5. *Functional decomposition of the Aδ-ERP elicited by the first stimulus (A, top-panel), by the average of stimuli 6-60 (B, middle panel), and of the concatenated Aδ-ERP elicited by stimulus 1 and 6-60 (C, bottom panel).* The top row of each panel shows the scalp topographies of the Independent Components (ICs), identified by pICA. The middle row of each panel shows the signals obtained by back-projecting each IC (thick colored waveforms) onto channel Cz. The original ERP waveforms at Cz is shown as a thin and grey line. The bottom row of each panel shows the contribution of each IC to the global field power.

Acknowledgments
FM and GDI were supported by a Wellcome Trust Strategic Award (COLL JLARAXR). GDI is additionally supported by a ERC Consolidator Grant (PAINSTRAT). AM is supported by an ERC Starting Grant (PROBING-PAIN). The authors declare no competing financial interests.

References

Bancaud J, Bloch V, Paillard J (1953) [Encephalography; a study of the potentials evoked in man on the level with the vertex]. Rev Neurol (Paris) 89:399-418.

Baumgartner U, Cruccu G, Iannetti GD, Treede RD (2005) Laser guns and hot plates. PAIN 116:1-3.

Beckmann CF, Smith SM (2004) Probabilistic independent component analysis for functional magnetic resonance imaging. IEEE Trans Med Imaging 23:137-152.

Bromm B, Treede RD (1984) Nerve fibre discharges, cerebral potentials and sensations induced by CO2 laser stimulation. Hum Neurobiol 3:33-40.

Burnham KP, Anderson DR (2002) Model Selection and Multimodel Inference, 2nd Edition: Springer-Verlag.

Byrne JH, Castellucci VF, Kandel ER (1978) Contribution of individual mechanoreceptor sensory neurons to defensive gill-withdrawal reflex in Aplysia. J Neurophysiol 41:418-431.

Carew TJ, Kandel ER (1973) Acquisition and retention of long-term habituation in Aplysia: correlation of behavioral and cellular processes. Science 182:1158-1160.

Castellucci V, Pinsker H, Kupfermann I, Kandel ER (1970) Neuronal mechanisms of habituation and dishabituation of the gill-withdrawal reflex in Aplysia. Science 167:1745-1748.

Courchesne E, Hillyard SA, Galambos R (1975) Stimulus novelty, task relevance and the visual evoked potential in man. Electroencephalogr Clin Neurophysiol 39:131-143.

Davis H, Osterhammel PA, Wier CC, Gjerdingen DB (1972) Slow vertex potentials: interactions among auditory, tactile, electric and visual stimuli. Electroencephalogr Clin Neurophysiol 33:537-545.

Fruhstorfer H (1971) Habituation and dishabituation of the human vertex response. Electroencephalogr Clin Neurophysiol 30:306-312.

Fruhstorfer H, Jarvilehto T, Soveri P (1969) Short-term habituation and dishabituation of the sensory evoked response in man. Acta Physiol Scand 76:14A-15A.

Fruhstorfer H, Soveri P, Jarvilehto T (1970) Short-term habituation of the auditory evoked response in man. Electroencephalogr Clin Neurophysiol 28:153-161.

Garcia-Larrea L, Frot M, Valeriani M (2003) Brain generators of laser-evoked potentials: from dipoles to functional significance. Neurophysiol Clin 33:279-292.

Greffrath W, Baumgartner U, Treede RD (2007) Peripheral and central components of habituation of heat pain perception and evoked potentials in humans. PAIN 132:301-311.

Hatem SM, Plaghki L, Mouraux A (2007) How response inhibition modulates nociceptive and non-nociceptive somatosensory brain-evoked potentials. Clin Neurophysiol 118:1503-1516.

Hu L, Mouraux A, Hu Y, Iannetti GD (2010) A novel approach for enhancing the signal-to-noise ratio and detecting automatically event-related potentials (ERPs) in single trials. Neuroimage 50:99-111.

Hu L, Valentini E, Zhang ZG, Liang M, Iannetti GD (2014) The primary somatosensory cortex contributes to the latest part of the cortical response elicited by nociceptive somatosensory stimuli in humans. Neuroimage 84:383-393.

Hu L, Liang M, Mouraux A, Wise RG, Hu Y, Iannetti GD (2011) Taking into account latency, amplitude, and morphology: improved estimation of single-trial ERPs by wavelet filtering and multiple linear regression. J Neurophysiol 106:3216-3229.

Huang G, Xiao P, Hung YS, Iannetti GD, Zhang ZG, Hu L (2013) A novel approach to predict subjective pain perception from single-trial laser-evoked potentials. Neuroimage 81:283-293.

Iannetti GD, Hughes NP, Lee MC, Mouraux A (2008) Determinants of laser-evoked EEG responses: pain perception or stimulus saliency? J Neurophysiol 100:815-828.

Iannetti GD, Leandri M, Truini A, Zambreanu L, Cruccu G, Tracey I (2004) Adelta nociceptor response to laser stimuli: selective effect of stimulus duration on skin temperature, brain potentials and pain perception. Clin Neurophysiol 115:2629-2637.

Jasper H, Sharpless S (1956) Habituation of the arousal reaction. Brain 79:655-680.

Jung TP, Makeig S, Humphries C, Lee TW, McKeown MJ, Iragui V, Sejnowski TJ (2000) Removing electroencephalographic artifacts by blind source separation. Psychophysiology 37:163-178.

Larsson LE (1956) The relation between the startle reaction and the non-specific EEG response to sudden stimuli with a discussion on the mechanism of arousal. Electroencephalogr Clin Neurophysiol 8:631-644.

Lee MC, Mouraux A, Iannetti GD (2009) Characterizing the cortical activity through which pain emerges from nociception. J Neurosci 29:7909-7916.

Legrain V, Guerit JM, Bruyer R, Plaghki L (2002) Attentional modulation of the nociceptive processing into the human brain: selective spatial attention, probability of stimulus occurrence, and target detection effects on laser evoked potentials. PAIN 99:21-39.

Liang M, Mouraux A, Chan V, Blakemore C, Iannetti GD (2010) Functional characterisation of sensory ERPs using probabilistic ICA: effect of stimulus modality and stimulus location. Clin Neurophysiol 121:577-587.

Makeig S, Jung TP, Bell AJ, Ghahremani D, Sejnowski TJ (1997) Blind separation of auditory event-related brain responses into independent components. Proc Natl Acad Sci U S A 94:10979-10984.

Mancini F, Beaumont AL, Hu L, Haggard P, Iannetti GD (2015) Touch inhibits subcortical and cortical nociceptive responses. PAIN 156:1936-1944.

Mancini F, Bauleo A, Cole J, Lui F, Porro CA, Haggard P, Iannetti GD (2014) Whole-body mapping of spatial acuity for pain and touch. Ann Neurol 75:917-924.

Moayedi M, Di Stefano G, Stubbs MT, Djeugam B, Liang M, Iannetti GD (2016) Nociceptive-Evoked Potentials Are Sensitive to Behaviorally Relevant Stimulus Displacements in Egocentric Coordinates. eNeuro 3.

Mountcastle VB (2005) Neural mechanisms of somatic sensation. Cambridge, Massachusetts: Harvard University press.

Mouraux A, Iannetti GD (2009) Nociceptive laser-evoked brain potentials do not reflect nociceptive-specific neural activity. J Neurophysiol 101:3258-3269.

Mouraux A, Iannetti GD, Plaghki L (2010) Low intensity intra-epidermal electrical stimulation can activate Adelta-nociceptors selectively. PAIN 150:199-207.

Mouraux A, De Paepe AL, Marot E, Plaghki L, Iannetti GD, Legrain V (2013) Unmasking the obligatory components of nociceptive event-related brain potentials. J Neurophysiol 110:2312-2324.

Rajan JJ, Rayner PJW (1997) Model order selection for the singular value decomposition and the discrete Karhunen-Loeve transform using a Bayesian approach. IEEE Proceedings on Vision, Images, and Signal Processing 144:116-123.

Ritter W, Vaughan HG, Jr., Costa LD (1968) Orienting and habituation to auditory stimuli: a study of short term changes in average evoked responses. Electroencephalogr Clin Neurophysiol 25:550-556.

Ronga I, Valentini E, Mouraux A, Iannetti GD (2013) Novelty is not enough: laser-evoked potentials are determined by stimulus saliency, not absolute novelty. J Neurophysiol 109:692-701.

Snyder E, Hillyard SA (1976) Long-latency evoked potentials to irrelevant, deviant stimuli. Behav Biol 16:319-331.

Spiegel J, Hansen C, Treede RD (1996) Laser-evoked potentials after painful hand and foot stimulation in humans: evidence for generation of the middle-latency component in the secondary somatosensory cortex. Neurosci Lett 216:179-182.

Sutton S, Braren M, Zubin J, John ER (1965) Evoked-potential correlates of stimulus uncertainty. Science 150:1187-1188.

Treede RD, Kief S, Holzer T, Bromm B (1988) Late somatosensory evoked cerebral potentials in response to cutaneous heat stimuli. Electroencephalogr Clin Neurophysiol 70:429-441.

Valentini E, Torta DM, Mouraux A, Iannetti GD (2011) Dishabituation of laser-evoked EEG responses: dissecting the effect of certain and uncertain changes in stimulus modality. J Cogn Neurosci 23:2822-2837.

Valentini E, Hu L, Chakrabarti B, Hu Y, Aglioti SM, Iannetti GD (2012) The primary somatosensory cortex largely contributes to the early part of the cortical response elicited by nociceptive stimuli. Neuroimage 59:1571-1581.

Wang AL, Mouraux A, Liang M, Iannetti GD (2010) Stimulus novelty, and not neural refractoriness, explains the repetition suppression of laser-evoked potentials. J Neurophysiol 104:2116-2124.

Wastell DG, Kleinman D (1980) Fast habituation of the late components of the visual evoked potential in man. Physiol Behav 25:93-97.

Wessel JR, Aron AR (2013) Unexpected events induce motor slowing via a brain mechanism for action-stopping with global suppressive effects. J Neurosci 33:18481-18491.

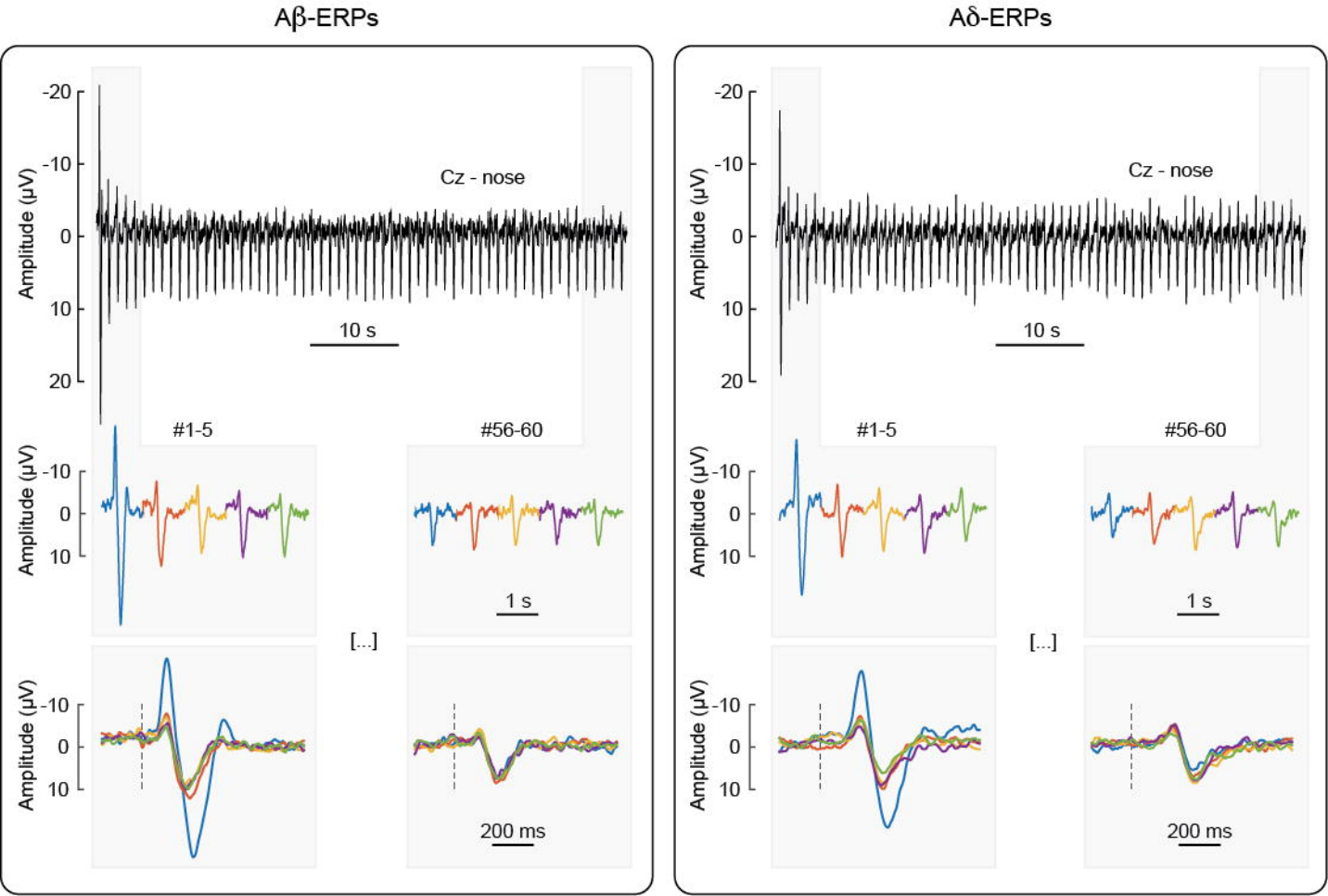
Aβ-ERPs
Aδ-ERPs
Cz - nose
Amplitude (μV)
-20
-10
0
10
20
10 s
#1-5
#56-60
1 s
[...]
200 ms

Trial #1

Trials #6-60

Ab ERPs

Ad ERPs

Trial #1

Trials #6-60

Amplitude (uV)

T-value

Cz-nose

Cc-Fz

N2

P2

N1

P4

P4(?)

122 ms

253 ms

98 ms

308 ms

532

210 ms

340 ms

183 ms

381 ms

127 ms

226 ms

113 ms

307 ms

202 ms

312 ms

161 ms

398 ms

25 uV

-25 uV

8 uV

-8 uV

22 uV

-22 uV

6 uV

-6 uV

4 uV

-4 uV

20 uV

-20 uV

10 uV

-10 uV

Latency (ms)

0 200 400 600 800

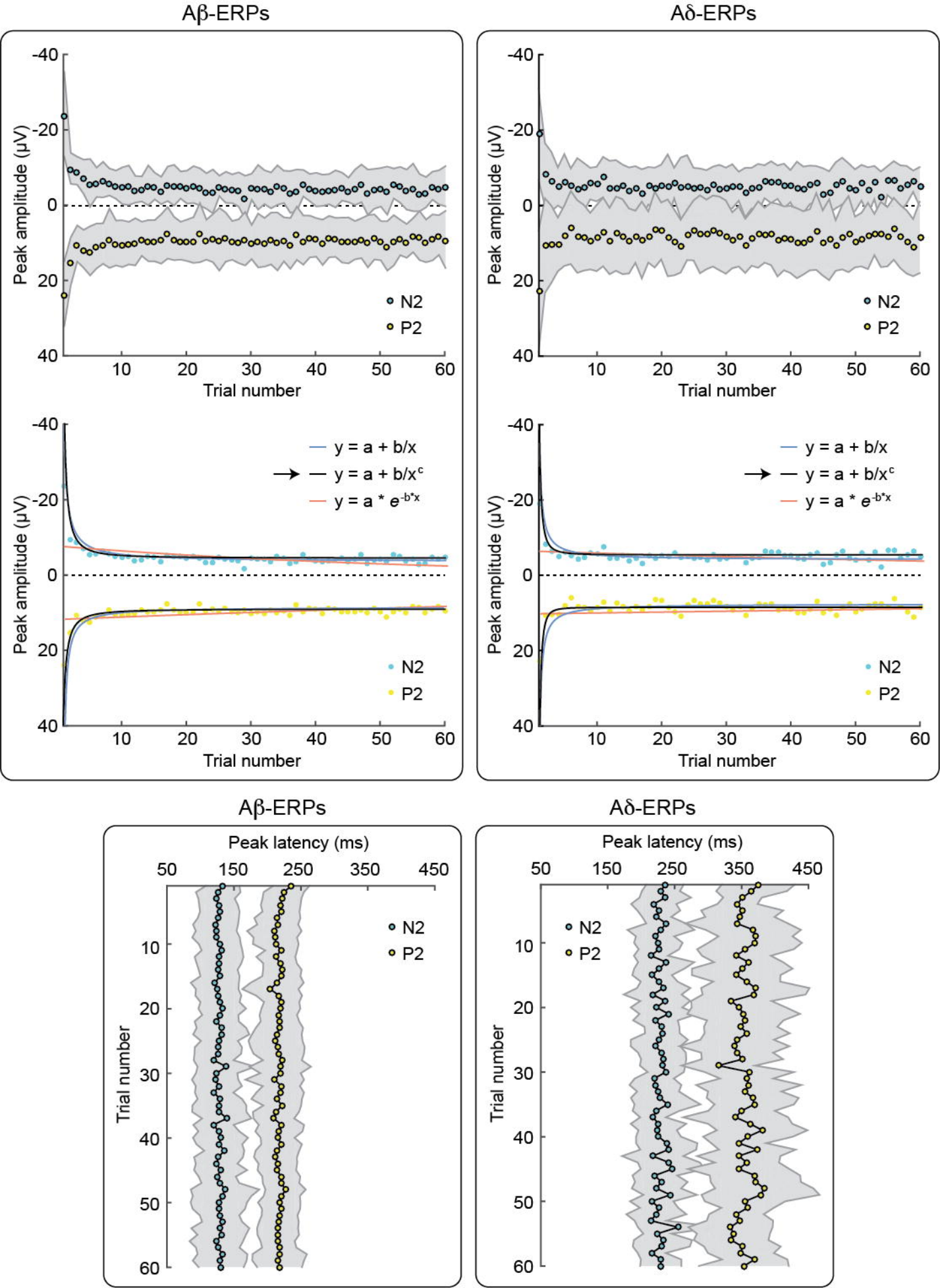
Aβ-ERPs
Aδ-ERPs
Peak amplitude (μV)
Trial number
N2
P2
y = a + b/x
y = a + b/x^c
y = a * e^-b*x
Peak latency (ms)